Iris Segmentation Using the Generalized Structure Tensor

Fernando Alonso-Fernandez and Josef Bigun
Halmstad University. Box 823. SE 301-18 Halmstad, Sweden
{feralo, Josef.Bigun}@hh.se

***Abstract*—We present a new iris segmentation algorithm based on the Generalized Structure Tensor (GST). We compare this approach with traditional iris segmentation systems based on Hough transform and integro-differential operators. Results are given using the CASIA-IrisV3-Interval database with respect to a segmentation made manually by a human expert. The proposed algorithm outperforms the baseline approaches, pointing out the validity of the GST as an alternative to classic iris segmentation systems. We also detect the cross positions between the eyelids and the outer iris boundary. Verification results using a publicly available iris recognition system based on 1D Log-Gabor wavelets are also given, showing the benefits of the eyelids removal step.**

I. Introduction

Biometrics has been receiving considerable attention over the last years due to the increasing demand for automatic person recognition. It refers to automatic recognition of an individual based on behavioral and/or physiological characteristics (e.g., fingerprints, face, iris, voice, etc.), which cannot be stolen, lost, or copied [1]. Among all biometric techniques, iris has been traditionally regarded as one of the most reliable and accurate biometric identification systems available [2], [3].

The iris is a ring around the pupil, surrounded by a white region called sclera (Figure 1). The pupil is generally darker than the iris and may have specular reflections due to light sources used in commercial acquisition systems. Iris analysis begins with the detection of the inner and outer iris boundaries. Early works make use of integro-differential operators, proposed by Daugman [4], and edge detection plus circular Hough transform, proposed by Wyldes [5]. They assume that iris boundaries can be modeled as circles. Much of the subsequent research has tried to improve the Wildes idea, such as the inherent computational burden of the Hough transform or the lack of enough edge points to define a circle [2]. Some works also deal with the problem of detecting eyelids occlusion or specular reflections. Current issues include the development of acquisition systems that allow larger distances between the subject and the sensor (typically meters), in which the apparent size of the iris and pupil will show much more variability, with an important presence of motion blur, inconsistent illumination or variation in subject gaze angles [6].

In this paper, we present a iris segmentation algorithm based on the Generalized Structure Tensor. By using circular filters sequentially, we first detect the inner (pupil) boundary and then, its center is used to refine the search of the outer (sclera) boundary. Since the pupil is generally darker than the iris, there will be a sharper transition which in principle will be easier to detect than the softer transition between the iris and the sclera. We compare our algorithm with traditional iris segmentation systems based on Hough transform and integro-differential operators. We also implement an eyelid detection step. We have used for our experiments the CASIA-IrisV3 Interval database, with 2,639 iris images from 249 contributors acquired in two sessions [7]. Reported results show the effectiveness of the proposed algorithm, outperforming the baseline systems. In addition, verification results of the proposed system using 1D Log-Gabor wavelets are given, showing the benefits of incorporating the eyelids detection step.

II. The 2D Structure Tensor

The Ordinary Structure Tensor (OST)

Given a gaussian smoothed image $I[p]$, the 2D *Ordinary* Structure Tensor [8] at a given pixel $p = [x, y]$ is the 2×2 matrix $S_w[p] = \sum_r w[r]\, S_o[p-r]$, where S_o is the matrix $S_o[p] = \begin{bmatrix} (f_x[p])^2 & f_x[p]\, f_y[p] \\ f_x[p]\, f_y[p] & (f_y[p])^2 \end{bmatrix}$. Index r ranges over coordinate pairs $\{-m...m\} \times \{-m...m\}$ and $w[r]$ is a weighting window centered at p (typically gaussian). The values $f_x[p]$, $f_y[p]$ are the estimated partial derivatives of $I[p]$ at pixel p, commonly implemented via convolutions with sampled gaussian-derivative filters. It can be shown that the following (complex) linear combinations of the real moments $m_{p,q}$ of the local power spectrum, which are the matrix elements of S_w, directly relate to the eigenvalues λ_1, λ_2 (and their corresponding eigenvectors e_1, e_2) of matrix $S_w[p]$ [9]:

$$I_{20} = (m_{11} - m_{22}) + i2m_{12} = (\lambda_1 - \lambda_2)\, e^{i2\varphi_{e_1}}$$
$$I_{11} = (m_{11} + m_{22}) = \lambda_1 + \lambda_2$$

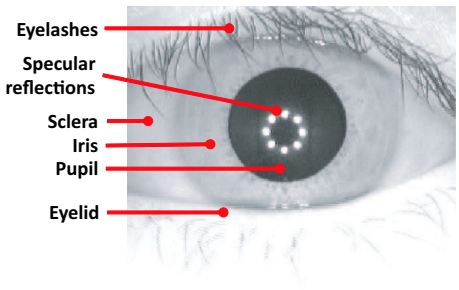

Fig. 1. Iris image with typical elements labeled.

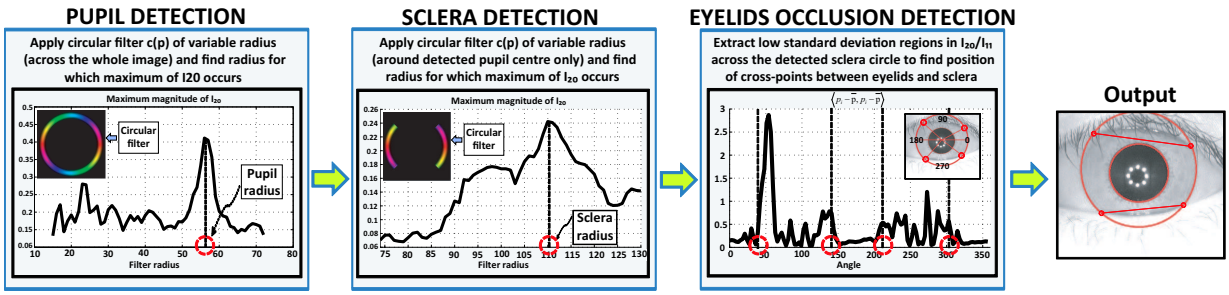

Fig. 2. System model for iris segmentation using the Generalized Structure Tensor.

Here i is the complex $\sqrt{-1}$. Hence, I_{20} (complex) and I_{11} (real) are the second order complex-moments of the power spectrum. They are also referred to as the (complex representation of the) structure tensor because they represent the ordinary structure tensor fully, with the advantage that eigenvalues and eigenvectors of S_w can be read out directly from I_{20}, I_{11}. This representation is increasingly preferred in fingerprint analysis as it conveniently allows a generalization of the structure tensor, offering efficient detection of singularities such as core and delta [10], [11]. It can be also demonstrated that $|I_{20}| \leq I_{11}$ (Schwartz inequality).

The Generalized Structure Tensor (GST)

Assuming that the inner/outer boundaries of the iris can be modeled as circles, they can be detected by means of the Generalized Structure Tensor, [9], which is essentially template matching in the tensor domain, and can be conveniently expressed using complex version of the structure tensor, i.e.

$$I_{20} = (\lambda_1 - \lambda_2)\, e^{i2\varphi_{e_1}} = \sum_p c\,(p)\,(f_x\,(p) + i f_y\,(p))^2$$

$$I_{11} = \lambda_1 + \lambda_2 = \sum_p |c\,(p)| \left|(f_x\,(p) + i f_y\,(p))^2\right|$$

where $c(p)$ is defined as the complex version of the structure tensor response of a circle[1]:

$$c\,(p) = e^{-i2\varphi_{e_1}} \left(x^2 + y^2\right)^{\gamma} e^{-\left(x^2+y^2\right)/\left(2\sigma_2^2\right)}$$

Here γ and σ_2 determine the radius of the circle and the precision of the filter (width of the circular boundary region). It can be shown that a high response in $|I_{20}|$ and zero argument of I_{20} is obtained at a point, if there are edges at the prescribed (same) distance from that point and there is an agreement in terms of local orientations (structure tensors) with those of a circle. It can also be shown that when this happens, the Schwartz inequality holds with equality, i.e. $|I_{20}| = I_{11}$.

III. Proposed System

We propose the use of the GST for iris segmentation following the process described next (summarized in Figure 2).

We first search for the pupil boundary with a circular filter of variable radius. The range of radius values is set manually, depending on the database (15-70 pixels for the CASIA-IrisV3 Interval). A peak in the response of $|I_{20}|$ will be obtained when the radius of the circular filter fits that of the pupil boundary, as can be seen in Figure 2, left. To improve detection, and to discard spurious peaks, a threshold to the argument of I_{20} is also imposed (+/-3 degrees in this work), so peaks with argument higher than the threshold are discarded.

After detecting the pupil boundary, another circular filter is used to search for the sclera boundary. The minimum radius of this filter is dynamically adjusted depending on the pupil radius, and the maximum radius is set to 140. For better accuracy, we search for the maximum value of $|I_{20}|$ only within a small region around the center of the pupil, since the two circles are assumed as being concentric to a certain extent [4]. In addition, to avoid possible occlusion by eyelids and eyelashes, we

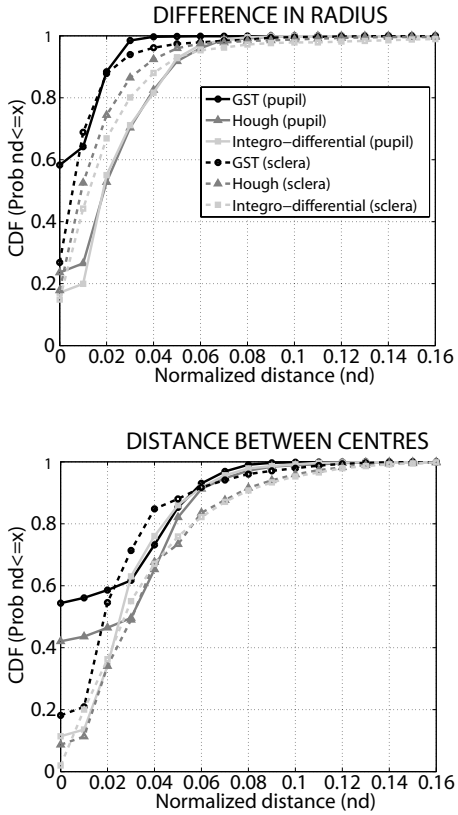

Fig. 3. Pupil and sclera segmentation accuracy (test set).

[1]In the ordinary structure tensor $c(p)$ is a Gaussian defining the extent of the local neighborhood.

use a circular filter in which top and bottom quarters are removed, as depicted in Figure 2. As before, the highest response of $|I_{20}|$ is obtained when the radius of the filter fits that of the sclera boundary, as seen in Figure 2. A threshold to the argument of I_{20} is also imposed here.

Finally, to detect the cross points between the eyelids and the sclera boundary, we sample the (complex) values of I_{20}/I_{11} across the sclera boundary with angle increments of 3 degrees, thus obtaining 120 samples in the 0-360 range. Given the vector $\mathbf{p} = (p_1, ..., p_i, ..., p_{120})$, we then compute for each sample p_i the (real) value $p'_i = \langle p_i - \overline{\mathbf{p}}, p_i - \overline{\mathbf{p}} \rangle$, with $\overline{\mathbf{p}}$ being the mean of $\mathbf{p}$. The resulting vector $\mathbf{p}' = (p'_1, ..., p'_i, ..., p'_{120})$ can be seen in Figure 2, third plot. As can be observed, regions with no eyelids occlusion exhibit small variance. The transition to regions of high variance is used to detect the position of the four cross points between the eyelids and the sclera (in case of low variance in an entire quadrant, we determine that there is no occlusion in it). This is because we expect that in regions of the sclera without occlusion, the Schwartz inequality between $|I_{20}|$ and I_{11} will tend to equality (i.e. agreement in terms of local orientations with those of a circle, as mentioned above). Therefore, the ratio $|I_{20}|/I_{11}$ will tend to one. On the other hand, in occluded regions of the sclera, the Schwartz inequality will not hold, and the ratio $|I_{20}|/I_{11}$ will exhibit an erratic behavior, with high variance.

After the segmentation process, we obtain the centre/radius of the two circles that model the boundaries of the iris region, and the coordinates of the four cross points (if exist) between the eyelids and the sclera. We also compute the straight line that crosses the upper/lower pair of cross points, and the iris region above/below the line is discarded.

IV. Experimental Framework

A. Database and Baseline Systems

We use the "Interval" set of the CASIA-IrisV3 database [7], with 2,639 images of 280×320 pixels (height×width) from 249 contributors acquired in 2 sessions with a close-up iris camera. The number of images per contributor and per session is not constant and not all the individuals have images of the two eyes. The number of different eyes is 396. The 249 subjects are further divided into a development set of 50 subjects (comprising 489 images) and a test set of 199 subjects (2166 images). The development set is used to find the optimal configuration of our segmentation system described in Section III, whereas the test set is used for validation.

As baseline segmentators, we use two freely available systems, one based on circular Hough transform, developed by Libor Masek [12], [13] and a second which is an implementation of the Daugman integro-differential operator [2]. The baseline matcher is also included in the Libor Masek source code. It is based on normalization of the iris region to polar coordinates using the Daugman's rubber sheet model [4], followed by a convolution with a 1D Log-Gabor wavelet plus phase binary quantization to four levels. Matching is done using the normalized Hamming distance, which incorporates noise masking, so that only significant (non-noisy) bits are used in calculating the distance between two iris templates.

[2]http://www.mathworks.com/matlabcentral/fileexchange/15652

B. Results

In Figure 3, we give the performance of our segmentation algorithm, as well as of the baseline segmentation systems. We have manually segmented all the images of the database with an script that allows the selection of three points in the pupil boundary and three points in the sclera boundary. With these two sets of points, we are able to compute the radius and the center of the iris and sclera circles. The performance of the automatic segmentation systems is then assessed by computing the difference between the automatic and the manually extracted radii of the circles (left plot of Figure 3) and the distance between the automatic and the manually extracted centers of the circles (right plot of Figure 3). Difference in radius and center distance are normalized by the pupil/sclera radius for size and dilation invariance. We observe that the proposed segmentation algorithm works better than the two baseline systems. Detected pupil and sclera circles using the GST algorithm are closer to the circles obtained with the manual segmentation. We also observe that sclera detection gives worse performance than pupil detection, pointing out our assumption that the iris/sclera transition is more difficult to detect.

To measure accuracy in eyelids cross-points detection, we have manually marked the cross-points of a group of images of the development set (one image per subject and per eye, resulting in 68 images). Performance is assessed by computing the difference between the angles along the sclera circle of the automatic and manually extracted cross-points. Results are depicted in Figure 4(a). We also report in Table I the percentage of False Positives (FP) and Negatives (FN). From Figure 4(a), we observe that accurate detection is more difficult in quadrants 1/2 (e.g. 50% or more of the images have an accuracy of 4 degrees in quadrants 3/4, but in quadrants 1/2 the percentage is below 30%). As observed in Figure 1, images in our database may have eyelashes in the upper quadrants, thus making more difficult the detection, which is not the case in the lower quadrants. On the other hand, according to results from Figure 4(a) and Table I, we cannot generalize if one quadrant is better that other (e.g. quadrant 1 has lower FP and FN). We speculate that it can be due to the presence of images from both left and right eyes. Adjusting our algorithm separately for each quadrant depending on the type of eye (right or left) could be a source of improvement.

Finally, in Figure 4(b), we give recognition results using the matcher described in Section IV-A. It can be observed that including the eyelid removal step results in a FRR decrease for any given value of the Hamming distance, and that the inter-class distance distribution is shifted towards smaller values, thus pointing out the utility of removing noisy regions of iris images.

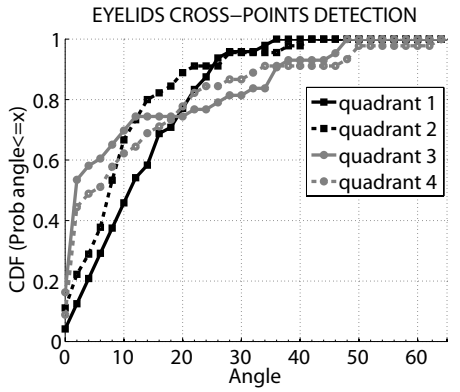

(a)

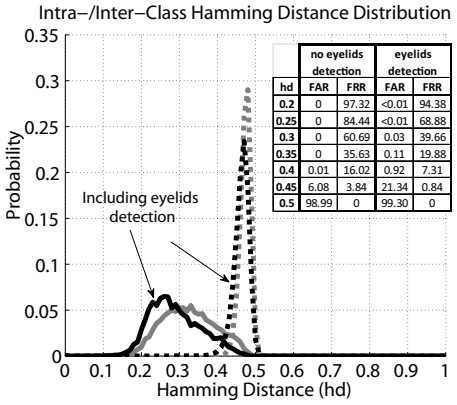

	no eyelids detection		eyelids detection	
hd	FAR	FRR	FAR	FRR
0.2	0	97.32	<0.01	94.38
0.25	0	84.44	<0.01	68.88
0.3	0	60.69	0.03	39.66
0.35	0	35.63	0.11	19.88
0.4	0.01	16.02	0.92	7.31
0.45	6.08	3.84	21.34	0.84
0.5	98.99	0	99.30	0

(b)

Fig. 4. **(a)**. Accuracy of eyelids cross-points detection. **(b)**. Inter- and intra-class Hamming distance distribution. False Accept and False Reject Rates at different working points are also given.

	Q1	Q2	Q3	Q4
False Positive	3.39	8.48	6.78	1.79
False Negative	5.09	10.17	13.56	8.48

TABLE I
ACCURACY OF EYELIDS CROSS-POINTS DETECTION
(Q1/Q2/Q3/Q4=QUADRANT 1/2/3/4).

V. CONCLUSIONS

A segmentation algorithm for iris images using the Generalized Structure Tensor has been proposed. We first search for the pupil boundary using a circular filter of variable radius and then, the center of the detected circle is used to refine the search of the sclera boundary with a second circular filter. We employ this sequential procedure since the pupil/iris transition is generally sharper than the iris/sclera transition, thus being easier to detect. Eyelid area is also computed by finding the cross position between the eyelids and the outer boundary of the iris. Using manual segmentation from a human expert as benchmark for our experiments, we have observed that pupil detection is correctly done in most of the database, but segmentation of the sclera results in worse performance. Apart from the softer transition between the iris and the sclera, another reason could be the occlusion of eyelids and eyelashes, since the database used in our experiments is composed mostly of oriental people. We also compare our system with popular segmentation algorithms based on circular Hough transform and integro-differential operators. Contrary to these baseline systems, our system exploits both the magnitude and the argument of filter responses. By using a complex filter (with local orientations), its response is penalized if there is disagreement of local orientations of the image with those of the filter (i.e. edges not forming a circle). As a result, our system outperforms the baseline systems tested here. In addition, verification results of the proposed system using 1D Log-Gabor wavelets are given. A performance improvement is observed when including the eyelid removal step. These results show the validity of our proposed approach and demonstrate that the Generalized Structure Tensor constitutes an alternative to classic iris segmentation approaches.

Future work includes improving the localization of eyelids and including detection of eyelashes. Eyelids can be modeled as circles, and therefore the algorithm presented in this paper can also be used for accurately finding their position. We will also evaluate the use of images acquired in less cooperative environments, e.g. the "Iris on the Move" project [14]. Currently this is one of the research hottest topics within the international biometric community [15], which drastically reduces the need of user's cooperation, and it will be another important source of future work.

ACKNOWLEDGMENT

Author F. A.-F. thanks the Swedish Research Council and the EU for for funding his postdoctoral research.

REFERENCES

[1] A.K. Jain, A. Ross, and S. Prabhakar, "An introduction to biometric recognition," *IEEE TCSVT*, vol. 14(1), Jan 2004.
[2] K.W. Bowyer, K. Hollingsworth, P.J. Flynn, "Image understanding for iris biometrics: a survey," *Elsevier CVIU*, vol. 110, 2007.
[3] E.M. Newton and P.J. Phillips, "Meta-analysis of third party evalutions of iris recognition," *NISTIR 7440*, 2007.
[4] John Daugman, "How iris recognition works," *IEEE TCSVT*, vol. 14, 2004.
[5] Richard P. Wildes, "Iris recognition: An emerging biometric technology," *Proc. IEEE*, vol. 85(9), 1997.
[6] J.R. Matey, R. Broussard, L. Kennell, "Iris image segmentation and sub-optimal images," *Elsevier IVC*, vol. 28(2), 2010.
[7] CASIA Iris Image Database, "http://biometrics.idealtest.org," .
[8] J. Bigun and G.H. Granlund, "Optimal orientation detection of linear symmetry," *Proc. ICCV*, June 1987.
[9] J. Bigun, *Vision with Direction*, Springer, 2006.
[10] Sharat Chikkerur, Nalini K. Ratha, "Impact of singular point detection on fingerprint matching performance," *Proc. AutoID*, 2005.
[11] K. Nilsson, J. Bigun, "Localization of corresponding points in fingerprints by complex filtering," *Patt. Rec. Letters*, vol. 24, 2003.
[12] Libor Masek, *Recognition of human iris patterns for biometric identification*, Ph.D. thesis, Western Australia Univ., 2003.
[13] L. Masek, P. Kovesi, "Matlab source code for a biometric identification system based on iris patterns," *School Computer Science and Software Engineering, Western Australia University*, 2003.
[14] J.R. Matey, O. Naroditsky, K. Hanna, R. Kolczynski, D. LoIacono, S. Mangru, M. Tinker, T. Zappia, and W.Y. Zhao, "Iris on the move: acquisition of images for iris recognition in less constrained environments," *Proc. IEEE*, vol. 94(11), 2006.
[15] NIST MBE, *Multiple Biometrics Evaluation - http://face.nist.gov/mbe*, 2009.